Nuclear resonance fluorescence in ^{240}Pu

B. J. Quiter, T. Laplace, B. A. Ludewigt, S. D. Ambers, B. L. Goldblum, S. Korbly, C. Hicks, and C. Wilson

Phys. Rev. C **86**, 034307 — Published 6 September 2012

DOI: 10.1103/PhysRevC.86.034307

Nuclear resonance fluorescence in ^{240}Pu

B.J. Quiter,[1] T. Laplace,[1,2] B.A. Ludewigt,[1] S.D. Ambers,[1,2] B.L. Goldblum,[1,2] S. Korbly,[3] C. Hicks,[3] and C. Wilson[3]

[1]*Lawrence Berkeley National Laboratory, Berkeley, California 94720, USA*
[2]*Berkeley Nuclear Research Center, University of California, Berkeley, California 94720, USA*
[3]*Passport Systems Incorporated, Billerica, Massachusetts 01862, USA*

(Dated: August 16, 2012)

Nuclear resonance fluorescence (NRF), a process by which a nucleus is excited by absorption of a specific quantum of energy and then de-excites via the emission of one or more γ rays, may be applied to non-destructively measure the isotopic composition of a sample. NRF excitations in ^{240}Pu were identified in the energy range of 2.1 to 2.8 MeV using a 3-MeV bremsstrahlung source. Utilizing high-purity germanium detectors at backward angles, nine resonances in ^{240}Pu were identified in this energy range. The measured integrated cross sections range from 29 to 104 eV·b. These resonances are of interest to nuclear structure physics and provide unique signatures for the assay of ^{240}Pu content for nuclear forensics, nuclear safeguards and counter-terrorism applications.

PACS numbers: 23.20.Lv, 25.20.Dc, 27.90.+b

I. INTRODUCTION

Nuclear resonance fluorescence (NRF) has received increased attention in recent years given its potential application in the non-destructive assay of fissile material content in spent fuel [1–4] and commercial cargo [5, 6]. In the NRF process, an excited nuclear state produced by the absorption of a photon emits one or more photons of specific energies upon de-excitation. By measuring the characteristic energies of an NRF state, one can uniquely identify and quantify the presence of specific isotopes. In order to utilize NRF in quantitative assay (e.g., verification of isotopic content in spent fuel at nuclear facilities, evaluation of isotopic content of interdicted nuclear material samples or cargo, etc.), the energies and strengths of the nuclear resonances of the isotopes of interest must be well known. The NRF spectrum of weapons-grade plutonium has been previously measured and the observed resonances were attributed to ^{239}Pu [7, 8]. Apart from this measurement, no NRF data had existed for other Pu isotopes.

Of particular interest is ^{240}Pu, which constitutes a significant fraction of the Pu mass in typical spent nuclear fuel [9], and if observed in spent fuel in $\lesssim$7% abundance may indicate weapons-grade plutonium production. As an even-even isotope, ^{240}Pu is expected to have significantly stronger NRF resonances than ^{239}Pu due to a decreased fragmentation of the dipole strength, and may prove more interesting in specific applications as a result. NRF excitations in ^{240}Pu were investigated and 18 γ-ray transitions, corresponding to nine ^{240}Pu NRF states, were identified in the energy range of 2.1 to 2.8 MeV. This measurement of ^{240}Pu NRF contributes to fundamental knowledge of nuclear structure and is relevant for nuclear security and safeguards applications.

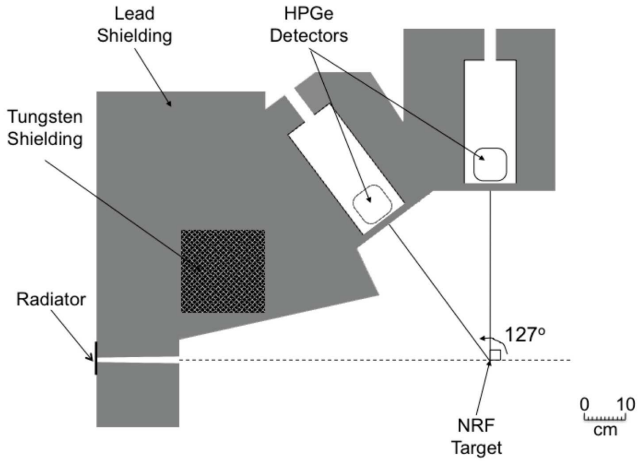

FIG. 1: Schematic of the experimental setup during active (beam-on) measurements. Additional Pb shielding was placed above and below the HPGe detectors (not shown).

II. EXPERIMENTAL METHOD

A 3-MeV electron beam produced by a Van de Graaff electron accelerator housed at the High Voltage Research Laboratory at the Massachusetts Institute of Technology was employed in the experiment. The average electron beam current was $\sim$40 μA. Bremsstrahlung photons were generated by impinging electrons on a 102-μm Au layer atop a 1-cm-thick water-cooled Cu backing ("radiator"). A 20-cm-thick Pb collimator (See Fig. 1) downstream of the radiator restricted the photon beam to a narrow cone with a half-angle of 1.8°. The ^{240}Pu target material was contained in a 30-μm-thick Al foil, sealed in a 2.8-cm-diameter Al container, and suspended in a sealed plastic bag 96.5 cm downstream of the radiator in the center of the photon beam.

Three high-purity germanium (HPGe) detectors were used to collect γ-ray spectra: one positioned at 90° and two at 127° (one atop the other), relative to the photon

TABLE I: Isotopic composition of the ^{240}Pu target calculated using a weighted least-squares approach for spherical and ellipsoidal sample geometries. The pear-shaped sample geometry, a best estimate based on digital radiograph data, was obtained as an average of the results for spherical and ellipsoidal sample geometries.

	$m_{^{239}\mathrm{Pu}}$ (10^{-2} g)	$m_{^{240}\mathrm{Pu}}$ (g)	$m_{^{241}\mathrm{Am}}$ (10^{-2} g)	$m_{^{237}\mathrm{U}}$ (10^{-10} g)	$m_{^{241}\mathrm{Pu}}$ (10^{-2} g)	m_{O} (10^{-1} g)	low-Z mass (g)
Sphere Model	2.4±0.6	4.71±0.03	2.55±0.03	3.83±0.09	1.29±0.04	6.39±0.05	0.8±0.1
Ellipsoid Model	2.2±0.6	4.62±0.03	2.46±0.03	3.61±0.07	1.14±0.03	6.26±0.05	0.9±0.1
Pear-Shaped Estimate	2.3±0.7	4.65±0.08	2.50±0.08	3.73±0.19	1.22±0.11	6.33±0.12	0.85±0.15

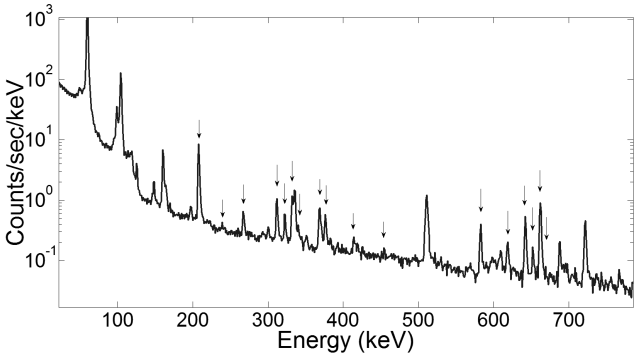

FIG. 2: Passive γ-ray spectrum of the ^{240}Pu target. The arrows indicate the 17 γ-ray peaks or multiplets used for determination of the target composition.

beam axis. As illustrated in Fig. 1, lead plates of 1.3-cm thickness were placed in front of the HPGe detectors during active measurements to attenuate the low-energy photon flux. The HPGe detector housing was positioned on a 7.6-cm layer of Pb atop a 7.6-cm-thick 80/20® aluminum table, with an additional 10.2 cm of Pb below the table and 28 cm of Pb above the HPGe detector housing. Detector energy and efficiency calibrations, the latter for the analysis of passive measurements, were performed as a function of γ-ray energy using ^{152}Eu and ^{137}Cs sources. Between 200 and 500 keV, γ rays from radioactive emissions from the target were also used to determine relative photon detection efficiencies.

A passive γ-ray spectrum of the ^{240}Pu target, an NRF spectrum of a blank target (i.e., a 30-μm-thick Al foil contained in a 2.8-cm-diameter Al cylinder) and an NRF spectrum of the ^{240}Pu target were obtained. Data were collected using Canberra Lynx® multichannel analyzers. High count rates (∼25 kHz) in the detector at 90° relative to the beam axis during active measurements resulted in poor energy resolution; thus, this detector was used for passive measurements only (See Sec. III). During active measurements, the count rates in the HPGe detectors at 127° relative to the beam axis were approximately $4-5$ kHz with a dead time of ∼6%.

III. TARGET COMPOSITION

Passive γ-ray spectroscopy (See Fig. 2) was used to determine the isotopic composition of the ^{240}Pu target. The target, as received, was reported to be a powder of ^{239}Pu, ^{240}Pu and ^{241}Pu in the oxide form, presumably PuO_2, contained in a 0.458 ± 0.001-g Al foil and sealed in a 5.358 ± 0.001-g Al container. Passive measurements suggested the presence of additional low-Z material. An X-ray image obtained during the bremsstrahlung irradiation of the target indicated that the PuO_2 was pear-shaped, sitting upright in the cylinder. A fitting procedure was employed to ascertain target composition by iteratively extracting sample parameters for both spherical and ellipsoidal geometries that best reproduced the relative γ-ray intensities measured during passive counting. A system of linear equations including 48 γ-ray peaks or multiplets at 17 different energies (denoted with arrows in Fig. 2) was evaluated:

$$\begin{pmatrix} \vdots & \vdots & \vdots & \vdots \\ \vdots & \vdots & \vdots & \vdots \\ I^i_{^{239}\mathrm{Pu}} & I^i_{^{240}Pu} & I^i_{^{241}Am} & I^i_{^{237}U} \\ \vdots & \vdots & \vdots & \vdots \\ \vdots & \vdots & \vdots & \vdots \end{pmatrix} \times \begin{pmatrix} m_{^{239}\mathrm{Pu}} \\ m_{^{240}\mathrm{Pu}} \\ m_{^{241}\mathrm{Am}} \\ m_{^{237}\mathrm{U}} \end{pmatrix} = \begin{pmatrix} \vdots \\ \vdots \\ N^i_C \\ \vdots \\ \vdots \end{pmatrix} \quad (1)$$

where $I^i_{^{\mathrm{A}}\mathrm{X}}$ represents the number of expected photons in a given peak or multiplet (denoted by the superscript i) per unit mass of the $^{\mathrm{A}}$X isotope [10], $m_{^{\mathrm{A}}\mathrm{X}}$ represents the corresponding mass, and N^i_C represents the number of counts measured in the ith peak or multiplet. The $I^i_{^{\mathrm{A}}\mathrm{X}}$ terms are the product of the number of photons emitted per unit mass of the isotope, the measured energy-dependent photopeak detection efficiency and the attenuation in the sample and container, the latter calculated using attenuation coefficients that exclude the contribution from coherent scattering obtained from the XCOM photon cross sections database [11]. Attenuation depends on the density and mass of low-Z material present in the sample; density was varied during the iterative process from 3 to 6 g/cm^3 in steps of 0.5 g/cm^3 and the mass of low-Z material in the sample was varied from 0 to 1.5 g in steps of 0.1 g.

The average attenuation of γ rays leaving the target in the direction of the HPGe detectors was calculated assuming both spherical and ellipsoidal sample geometries and these were averaged to approximate the pear-shaped

target. The masses of each isotope, $m_{^A\mathrm{X}}$, were determined by a weighted least-squares regression analysis of Eq. 1. The density of the sample was determined to be $4.25\pm0.18\,\mathrm{g/cm^3}$ and the deduced isotopic composition of the sample is given in Table I. To provide a conservative estimate due to ambiguity in the sample geometry, the reported mass uncertainties for the pear-shaped target geometry were made to encompass the statistical error ranges of the spherical and ellipsoidal models.

To verify the attenuation calculated using the analytical model, MCNPX [12] simulations were performed whereby the sample was treated as a spherical source of low-energy mono-directional photons. The relative rate of photon incidence upon the simulated detector surface as a function of γ-ray energy, indicative of the self-attenuation of photons in the sample, was generated with 0.02% statistical uncertainty and compared to that obtained from the analytical model. Agreement between the simulation and the analytical model was reached to within 0.5% over the range of γ-ray energies relevant for the assessment. These simulations were also used to estimate the component of systematic uncertainty arising from calculation of photon attenuation in the determination of the ^{240}Pu NRF integrated cross sections.

IV. RESULTS AND UNCERTAINTIES

For even-even nuclei with $I^\pi = 0^+$ ground states (e.g., ^{240}Pu), photon excitation typically results in the population of $J^\pi = 1^\pm$ and $J^\pi = 2^+$ levels, the latter being less probable. The NRF states observed in this work all appeared to be characterized by two peaks in the γ-ray spectrum that correspond to transitions to the ground and first excited state at 42.8 keV ($\mathrm{J}^\pi = 2^+$). The partial widths for these transitions are denoted by Γ_0 and Γ_1, respectively, or more generally as Γ_i, where i is the index of the decay modes of the level. The NRF spectrum of the ^{240}Pu target (solid line) and radioactive target background spectrum (dashed line) are shown in Fig. 3. The integrated cross sections of the ^{240}Pu NRF transitions, whose energies are indicated with arrows in Fig. 3, were determined relative to the ^{27}Al resonance at $E_{\mathrm{Al}} = 2212.0$ keV, denoted by the asterisk, whose integrated cross section has been measured as $\int\sigma_{\mathrm{Al}}dE = 18.00\pm0.33$ eV·b [13]. The intense γ-ray transition present in both the NRF and background spectra at 2614.5 keV is attributed to decay of ^{208}Tl. The circles at 2221.3 keV and 2601.5 keV indicate relatively low-intensity regions in the radioactive background spectrum upon which NRF ^{240}Pu γ rays corresponding to transitions to the first excited state of ^{240}Pu appeared to be present.

The integrated cross section for a particular NRF transition in ^{240}Pu, $\frac{\Gamma_i}{\Gamma}\int\sigma_{\mathrm{Pu}}(E_\gamma)dE$, was obtained relative to

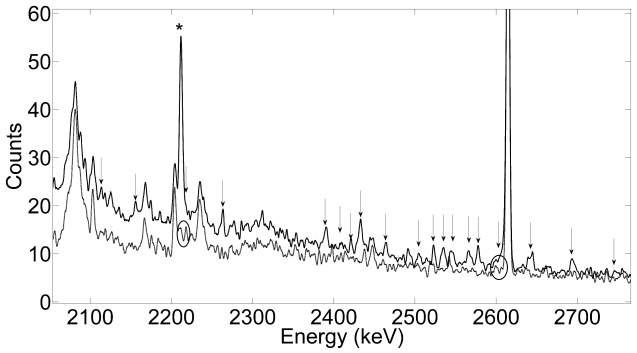

FIG. 3: NRF spectrum of the ^{240}Pu target (solid line) and radioactive target background (dashed line) in the γ-ray energy range from 2 to 2.8 MeV. The arrows indicate the 18 γ rays corresponding to the nine populated NRF states. The asterisk denotes the ^{27}Al resonance at 2212.0 keV and the circles indicate relatively low-intensity regions in the background spectrum upon which ^{240}Pu γ rays are expected.

the 2212-keV ^{27}Al resonance, $\int\sigma_{\mathrm{Al}}dE$, as:

$$\frac{\Gamma_i}{\Gamma}\int\sigma_{\mathrm{Pu}}(E_\gamma)dE = \frac{\int\sigma_{\mathrm{Al}}dE\,N_{\mathrm{Pu}}n_{\mathrm{Al}}W_{\mathrm{Al}}(\theta)\epsilon_{\mathrm{Al}}\Phi_{\mathrm{Al}}\lambda_{\mathrm{Al}}}{N_{\mathrm{Al}}n_{\mathrm{Pu}}W_{\mathrm{Pu}}(\theta)\epsilon(E_\gamma)\Phi(E)\lambda_{\mathrm{Pu}}(E,E_\gamma)}, \quad (2)$$

where N_{Pu} and N_{Al} are the dead-time-corrected number of counts in the full-energy peak for each NRF transition and the fiducial ^{27}Al resonance; n_{Pu} and n_{Al} are the number of ^{240}Pu and ^{27}Al atoms in the sample; $W_{\mathrm{Al}}(\theta)$ and $W_{\mathrm{Pu}}(\theta)$ are the angular correlation functions of the scattered photons with respect to the incoming photon beam for the ^{27}Al and ^{240}Pu NRF states; ϵ is the photopeak detection efficiency as a function of γ-ray energy, E_γ; Φ is the bremsstrahlung flux at the energy of the NRF state, E; and λ is the photon attenuation within the sample, a function of both E_γ and E, which may include substantial resonant attenuation for γ rays at energies corresponding to resonances with larger integrated cross sections. Peak areas were determined via curve fitting with an asymmetrically-modified Gaussian-plus-exponential functional form above a linear background [14]. Local baselines were fit as linear functions and subtracted before peak characterization was performed. The angular correlation functions for the ^{240}Pu resonances, $W_{\mathrm{Pu}}(\theta)$, for spin sequences of 0-1-0 are not isotropic, but have values close to unity over the angular range subtended by the detector. Conversely, the values of $W_{\mathrm{Pu}}(\theta)$ for the spin sequences of 0-1-2 and the angular correlation function for the ^{27}Al resonance, $W_{\mathrm{Al}}(\theta)$, are very nearly isotropic. As such, the ratio $W_{\mathrm{Al}}(\theta)/W_{\mathrm{Pu}}(\theta)$ is assumed to be unity. The energy-dependence of the detection efficiency and bremsstrahlung flux were estimated using MCNPX simulations, described in more detail below. Values for photon attenuation in the sample, λ, were calculated using an iterative finite element method, assuming spherical sample geometry, and included attenuation of both the incident bremsstrahlung and emitted NRF photons.

TABLE II: ^{240}Pu NRF transition energies and integrated cross sections. The ratio of the reduced transition probabilities for transitions to the first excited and ground states, R_{exp}, was deduced from the experimental data as described in the text. Total integrated cross sections are given with associated statistical uncertainties, followed by systematic uncertainties.

Energy (keV)	$\frac{\Gamma_i}{\Gamma}\int\sigma dE$ (eV·b)	R_{exp}	$\int\sigma dE$ (eV·b)
2113.1±0.6	19.6±4.3	1.41±0.44	34.4±5.4±1.8
2155.6±0.4	14.8±3.5		
2221.3±0.8	8.3±4.8	0.42±0.26	29.4±6.7±1.5
2263.3±0.4	21.0±4.8		
2390.4±0.3	35.8±6.0	0.56±0.10	103.7±7.7±4.9
2433.2±0.3	67.9±6.2		
2421.2±0.4	19.1±4.1	0.85±0.22	42.7±5.4±2.0
2464.2±0.3	23.6±3.9		
2505.3±0.4	23.8±6.5	1.40±0.55	41.8±8.1±3.8
2547.4±0.6	17.9±5.6		
2523.3±0.4	39.1±5.7	1.14±0.21	75.2±6.7±7.1
2566.4±0.4	36.1±6.1		
2534.9±0.4	39.0±6.0	1.04±0.17	78.3±6.7±8.2
2577.5±0.4	39.3±6.5		
2601.5±0.5	24.2±7.0	0.58±0.17	68.3±9.1±10.2
2644.5±0.3	44.1±9.6		
2693.8±0.3	37.5±8.4	1.70±0.50	60.7±8.3±9.5
2736.0±0.5	23.2±6.8		

TABLE III: Energy-dependent components of the statistical and systematic uncertainty in the ^{240}Pu NRF integrated cross sections. Stated statistical uncertainty values, σ_{stat}, include error associated with peak fitting.

Energy	σ_{stat}	σ_{syst} (%)			
(keV)	(%)	$\frac{\epsilon_{Al}}{\epsilon(E_\gamma)}$	$\frac{\Phi_{Al}}{\Phi(E)}$	$\lambda_{\rm Pu}(E,E_\gamma)$	Total
2113	21.3	0.33	2.6	1.32	5.32
2156	22.8	0.19	2.6	1.29	5.64
2221	57.3	0.03	2.1	1.47	5.10
2263	22.3	0.17	2.1	1.44	5.45
2390	16.0	0.59	1	1.48	4.82
2433	7.5	0.74	1	1.46	5.20
2421	20.9	0.70	0.7	1.07	4.67
2464	15.7	0.84	0.7	1.05	5.06
2505	25.6	0.98	7.6	1.70	8.99
2547	30.0	1.12	7.6	1.68	9.20
2523	11.3	1.04	8.0	1.81	9.38
2566	14.0	1.18	8.0	1.78	9.59
2535	11.5	1.08	9.1	2.02	10.4
2578	12.6	1.22	9.1	1.99	10.6
2602	25.0	1.30	14.1	2.08	14.9
2645	15.6	1.44	14.1	2.05	15.1
2694	16.0	1.51	14.6	2.36	15.5
2736	25.0	1.75	14.6	2.32	15.6

The energies and integrated cross sections of the 18 γ rays observed are given in Table II. No transitions to states other than the ground and first excited states were observed in this work. Therefore, as typical of NRF measurements on even-even nuclei [15–17], the total integrated cross section of the NRF state is assumed to be equal to the sum of the integrated cross sections for transitions to the ground and first excited states (i.e., for each observed state, $\Gamma = \Gamma_0 + \Gamma_1$).

A detailed uncertainty analysis was performed and results are provided in Table III. The error in the determination of the total integrated cross sections is dominated by the statistical uncertainty for states with $E < 2550$ keV. The statistical error is based solely on the fitted number of counts attributed to each ^{240}Pu NRF transition. The sources of systematic error in the measurement include the uncertainty in the number of ^{240}Pu and ^{27}Al atoms in the sample (1.72% and <0.1%, respectively), the uncertainty in the number of counts in the ^{27}Al NRF peak (3.5%), the uncertainty in the reference cross section (1.8%), the deviation from unity of the ratio of the angular correlation functions for the ^{27}Al and ^{240}Pu transitions (2.2% and 1.1%, for spin sequences of 0-1-0 and 0-1-2, respectively), the uncertainty in the attenuation of resonant incoming and resultant outgoing photons by the target, and the energy-dependent relative uncertainties in the γ-ray detection efficiency of the HPGe detectors and the intensity of the bremsstrahlung flux. The uncertainty in photon attenuation was estimated by recalculating photon attenuation using the 1-σ range of the previously-measured ^{27}Al and deduced ^{240}Pu integrated cross sections (see Sec. III). This method resulted in a 0.1% uncertainty for $\lambda_{\rm Al}$ and uncertainties ranging from 1.1 to 2.4% for values of $\lambda_{\rm Pu}$.

The uncertainty in the detection efficiency at the energy of each observed transition, E_γ, relative to the simulated detection efficiency at $E_{\rm Al}$, was estimated by conservatively assuming twice the uncertainty obtained in a previous work devoted to examining the sensitivity of efficiencies obtained via Monte Carlo simulations to HPGe detector parameters [18]. As shown in Table III, this resulted in estimated errors of ϵ at each E_γ, relative to the simulated detection efficiency at $E_{\rm Al}$, that increased linearly with $|E_\gamma - E_{\rm Al}|$, and reached a maximum of 1.75% at 2736 keV.

The intensity of bremsstrahlung photons at E, relative to the intensity at $E_{\rm Al}$, was initially estimated by simulating electron-induced bremsstrahlung emission from the radiator using MCNPX. Bremsstrahlung production cross sections in MCNPX are based upon tabulations by Seltzer and Berger [19], which utilized theoretical predictions for electron energies above 50 MeV and below 2 MeV, and interpolated as a function of E/E_e to provide cross sections at intermediate electron energies. The error associated with this interpolation scheme for 3 MeV electrons was quantitatively estimated for the NRF state energies, E, as described below, and an energy-dependent correction to the ratio, $\Phi(E)/\Phi_{\rm Al}$, was subsequently applied.

MCNPX simulations were compared to experimental measurements of forward-directed bremsstrahlung induced from electrons with energies of $E_e = 1.7$ and

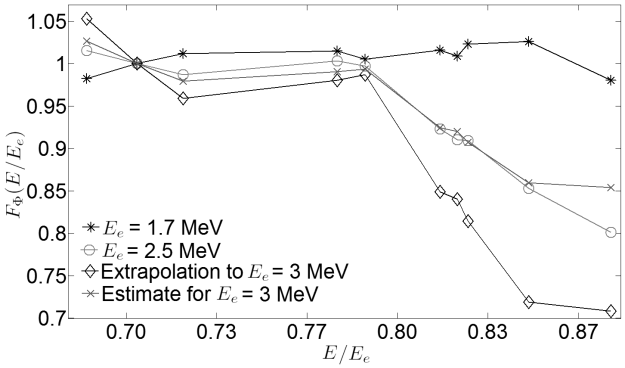

FIG. 4: The relative flux ratio, $F_\Phi(E/E_e)$, given in Eq. 3, was determined by comparing measured bremsstrahlung spectra at E_e = 1.7 and 2.5 MeV with MCNPX simulations of the measurements as functions of E/E_e. These values were extrapolated for E_e = 3.0 MeV (indicated by '$\diamond$'). Values representing half of the deviation from unity of the E_e = 3.0 MeV extrapolated values (indicated by '$\times$') were used to scale the flux ratio in Eq. 2 and a corresponding systematic error, given in Table III, was assigned. The lines through the data points are guides to the eye.

2.5 MeV impinging on a Au radiator [20]. To estimate the error associated with MCNPX-predicted bremsstrahlung intensity at E, relative to $E_{\rm Al}$, each measured and simulated flux, $\Phi_{exp}(E)$ and $\Phi_{\rm MC}(E)$, respectively, were normalized at $E_{\rm Al}$ and compared as functions of E/E_e. We define the relative flux ratio as

$$F_\Phi(E/E_e) = \frac{\Phi_{\rm MC}(E/E_e)/\Phi_{\rm MC}(E_{\rm Al}/E_e)}{\Phi_{exp}(E/E_e)/\Phi_{exp}(E_{\rm Al}/E_e)}, \qquad (3)$$

where a deviation of $F_\Phi(E/E_e)$ from unity is indicative of systematic disagreement between the shape of the bremsstrahlung spectrum predicted by MCNPX and that experimentally measured. For both E_e = 1.7 and 2.5 MeV, the quantity $F_\Phi(E/E_e)$ was calculated for each value of E/E_e that corresponded to the observed ^{240}Pu NRF states with E_e = 3.0 MeV, as shown in Fig. 4. For E_e = 1.7 MeV, the agreement is quite good, as expected, whereas at E_e = 2.5 MeV disagreement increases with E/E_e to ∼15% at E/E_e = 0.88. The values of $F_\Phi(E/E_e)$ were extrapolated to E_e = 3 MeV and are also plotted in Fig. 4. This extrapolation suggests that the MCNPX simulations underestimate the flux at E = 2736 keV, relative to that at $E_{\rm Al}$, by 29%. To address this, the MCNPX-predicted values of $\Phi(E)/\Phi_{\rm Al}$ in Eq. 2 were modified to half of this estimated deviation, and the systematic uncertainties associated with the difference between actual and MCNPX-predicted relative bremsstrahlung intensities, given in Table III, were also assumed to be half the predicted deviation.

V. DISCUSSION

The γ-ray transition at 2464.2(3) keV in this work is within $\pm1\sigma$ of the 2464.60(30) keV transition attributed to ^{239}Pu by Bertozzi, *et al.* [8]. As shown in Table II, the ^{240}Pu transition was associated with a transition to the first excited state of ^{240}Pu at 2421.2(4) keV. Bertozzi, *et al.*, also identified transitions at 2423.48(22) keV and 2431.66(25) keV. However, given the agreement with the ^{240}Pu transitions at 2421.2(4) keV and 2433.2(3) keV observed in this work, it is also possible that these γ rays resulted from ^{240}Pu isotopic contamination of the ∼93% pure ^{239}Pu target utilized in the Bertozzi, *et al.*, experiment.

According to the Alaga rules [21, 22], the ratio, R, of the reduced transition probabilities, B, for transitions to the first excited and ground states is given by:

$$R = \frac{B(1^\pi \rightarrow 2^+)}{B(1^\pi \rightarrow 0^+)} = \begin{cases} 1/2 & K = 1 \\ 2 & K = 0 \end{cases}, \qquad (4)$$

where K is the projection of the total angular momentum vector of the resonant state on the nuclear symmetry axis. Ratios that deviate from the theoretical values indicate K-mixing of the resonant states. The reduced transition probability is related to the decay width of the transition [23]. Assuming only dipole transitions, the ratio of the reduced transition probabilities for transitions to the first excited and ground states can be deduced from the experimentally-determined integrated cross sections:

$$R_{exp} = \frac{\Gamma_1}{\Gamma_0}\left(\frac{E_0}{E_1}\right)^3 = \frac{I_1}{I_0}\left(\frac{E_0}{E_1}\right)^3, \qquad (5)$$

where I_1 and I_0 represent the integrated cross sections for transitions to the first excited and ground states, and E_1 and E_0 are the corresponding transition energies. The empirical ratios are given in the third column of Table II with associated statistical uncertainties.

The R_{exp} values for approximately 160 levels for various actinide nuclei were recently compiled and many R_{exp} values were found to lie between 1/2 and 2, indicative of the K-mixing expected in high level-density regions [17]. Of the nine R_{exp} values obtained in this work, three may agree with a value of 0.5 and one with a value of 2, within estimated uncertainty. Thus, five levels (i.e., 2155.6 keV, 2464.2 keV, 2547.4 keV, 2566.4 keV and 2577.5 keV) exhibit R_{exp} values that violate the Alaga rules within $\pm1\sigma$, implying admixing of different values of K for these resonances.

VI. CONCLUSIONS

Eighteen γ rays corresponding to nine NRF states in ^{240}Pu have been discovered in the 2.1 to 2.8 MeV energy range. The strengths of these resonances lie between approximately 29 and 104 eV·b, significantly larger than

those measured for ^{239}Pu. The strongest resonances in this work are comparable in strength to the strongest resonances observed for ^{238}U [16, 17, 24]. These measurements contribute to the knowledge of actinide nuclear structure and support the evaluation of NRF as a non-destructive assay method for plutonium isotopes in nuclear nonproliferation and safeguards applications. Future work will include a measurement of the dipole response of ^{240}Pu to polarized photons.

Acknowledgments

This work was supported by the Office of Nonproliferation and Verification Research and Development, National Nuclear Security Administration, US Department of Energy under Contract No. DE-AC02-05CH11231. This work was also supported by the Berkeley Nuclear Research Center (BNRC) through the 00F8F4 University of California Lab Fees Research Program.

[1] B.J. Quiter, B.A. Ludewigt, V.V. Mozin, and S.G. Prussin, IEEE Trans. Nucl. Sci. Nuclear Science, **58**, 400 (2011).
[2] S.J. Tobin, J.L. Conlin, L.G. Evans and J. Hu, Los Alamos National Laboratory Report No. LA-UR-10-06243, 2010.
[3] B. Quiter, B. Ludewigt, V. Mozin and S.G. Prussin, in *Proceedings of the Institute on Nuclear Materials Management, 50th Annual Meeting, Tuscon, 2009.*
[4] S.J. Tobin, N.P. Sandoval, M.L Fensin, S.Y. Lee, B.A. Ludewigt, H.O Menlove, B.J. Quiter, A. Rajasingum, M.A. Schear, L.E. Smith, *et al.*, Los Alamos National Laboratory Report No. LA-UR-09-03748, 2009.
[5] W. Bertozzi and R.J. Ledoux, Nucl. Instrum. Meth. B **241**, 820 (2005).
[6] C.A. Hagmann, J.M. Hall, M.S. Johnson, D.P. McNabb, J.H. Kelley, C. Huibregtse, E. Kwan, G. Rusev and A.P. Tonchev, J. Appl. Phys. **106**, 084901 (2009).
[7] M. Johnson, D.P. McNabb and E.B. Norman, Lawrence Livermore National Laboratory Report No. UCRL-TR-228387, 2007.
[8] W. Bertozzi, J.A. Caggiano, W.K. Hensley, M.S. Johnson, S.E. Korbly, R.J. Ledoux, D.P. McNabb, E.B. Norman, W.H. Park and G.A. Warren, Phys. Rev. C **78**, 041601(R) (2008).
[9] J.R. Phillips, in *Passive Nondestructive Assay of Nuclear Materials*, edited by D. Reilly, N. Ensslin, H. Smith, Jr. and S. Kreiner (United States Nuclear Regulatory Commission, Washington, 1991).
[10] *Table of Radioactive Isotopes*, edited by E. Browne, R.B. Firestone and V.S. Shirley (John Wiley & Sons, New York, 1986).
[11] M.J. Berger, J.H. Hubbell, S.M. Seltzer, J.S. Coursey, and D.S. Zucker, XCOM: Photon cross sections database, Physics Laboratory, National Institute of Standards and Technology Report No. NBSIR 87-3597, 1998.
[12] D.B. Pelowitz, ed., MCNPX User's Manual, Version 2.6.0, Los Alamos National Laboratory Report No. LA-CP-07-1473, 2008.
[13] N. Pietralla, I. Bauske, O. Beck, P. von Brentano, W. Geiger, R.-D. Herzberg, U. Kneissl, J. Margraf, H. Maser, H.H. Pitz, *et al.*, Phys. Rev. C **51**, 1021 (1995).
[14] J.T. Routti and S.G. Prussin, Nucl. Instrum. Meth. **72**, 125 (1969).
[15] A. Zilges, P. von Brentano, R.-D. Herzberg, U. Kneissl, J. Margraf, H. Maser, N. Pietralla and H.H. Pitz, Phys. Rev. C **52**, R468 (1995).
[16] B.J. Quiter, B.A. Ludewigt , V.V. Mozin, C. Wilson and S. Korbly, Nucl. Instrum. Meth. B **269**, 1130 (2011).
[17] S.L. Hammond, A.S. Adekola, C.T. Angell, H.J. Karwowski, E. Kwan, G. Rusev, A.P. Tonchev, W. Tornow, C.R. Howell and J.H. Kelley, Phys. Rev. C **85**, 044302 (2012).
[18] M.A. Ludington and R.G. Helmer, Nucl. Instrum. Meth. A **446**, 506 (2000).
[19] S.M. Seltzer and M.J. Berger, Nucl. Instrum. Meth. B **12**, 95 (1985).
[20] D.H. Rester and W.E. Dance, Phys. Rev. **161**, 85 (1967).
[21] G. Alaga, K. Alder, A. Bohr and B.R. Mottelson, Mat. Fys. Medd. Dan. Vid. Selsk. **29**, 1 (1955).
[22] E. Hammarén, P. Heikkinen, K.W. Schmid and A. Faessler, Nucl. Phys. A **541**, 226 (1992).
[23] U. Kneissl, H.H. Pitz and A. Zilges, Prog. Part. Nucl. Phys. **37**, 349 (1996).
[24] R.D. Heil, H.H. Pitz, U.E.P. Berg, U. Kneissl, K.D. Hummel, G. Kilgus, D. Bohle, A. Richter, C. Wesselborg and P. von Brentano, Nucl. Phys. A **476**, 39 (1988).